

# Turbulent shear flow over fast-moving waves

By J. E. COHEN<sup>1</sup>† AND S. E. BELCHER<sup>2</sup>

<sup>1</sup>Department of Applied Mathematics and Theoretical Physics, University of Cambridge,  
Cambridge, CB3 9EW, UK

<sup>2</sup>Department of Meteorology, University of Reading, Reading RG6 6BB, UK

(Received 2 April 1998 and in revised form 2 December 1998)

We divide the interaction between wind and ocean surface waves into three parameter regimes, namely slow, intermediate and fast waves, that are distinguished by the ratio  $c/u_*$  ( $c$  is the wave phase speed and  $u_*$  is the friction velocity in the wind). We develop here an analytical model for linear changes to the turbulent air flow caused by waves of small slope that is applicable to slow and to fast waves. The wave-induced turbulent shear stress is parameterized here with a *damped mixing-length model*, which tends to the mixing-length model in an inner region that lies close to the surface, and is then damped exponentially to zero in an outer region that lies above the inner region. An adjustable parameter in the damped mixing-length model controls the rate of decay of the wave-induced stress above the inner region, and shows how the results vary from a model with no damping, which corresponds to using the mixing-length model throughout the flow, to a model with full damping, which, following previous suggestions, correctly represents rapid distortion of the wave-induced turbulence in the outer region.

Solutions for air flow over fast waves are obtained by analysing the displacement of streamlines over the wave; they show that fast waves are damped, thereby giving their energy up to the wind. There is a contribution to this damping from a counterpart of the non-separated sheltering mechanism that gives rise to growth of slow waves (Belcher & Hunt 1993). This sheltering contribution is smaller than a contribution from the wave-induced surface stress working against the orbital motions in the water. Solutions from the analysis for both slow and fast waves are in excellent agreement with values computed by Mastenbroek (1996) from the nonlinear equations of motion with a full second-order closure model for the turbulent stresses. Comparisons with data for slow and intermediate waves show that the results agree well with laboratory measurements over wind-ruffled paddle-generated waves, but give results that are a factor of about two smaller than measurements of purely wind-generated waves. We know of no data for fast waves with which to compare the model. The damping rates we find for fast waves lead to e-folding times for the decay of the waves that are a day or longer. Although this wind-induced damping of fast waves is small, we suggest that it might control low-frequency waves in a fully-developed sea.

---

## 1. Introduction

There has been renewed interest in recent years in studying the ways that the wind blowing over the ocean interacts with surface waves. This renewed interest has been catalysed by applying the understanding of the role of turbulent stresses in flow over

† Present address: Silsoe Research Institute, Wrest Park, Silsoe, Bedford, MK45 4HS, UK.

hills (e.g. Hunt, Leibovich & Richards 1988; Belcher, Newley & Hunt 1993) to understand flow over waves. Turbulent stresses in the air flow over waves lead to a *sheltering* in the lee of the wave, whereby streamlines are displaced asymmetrically about the wave crest and wind speeds in the lee of the wave are reduced. This mechanism is related to the mechanism put forward by Jeffreys (1925), who assumed that the air flow separates in the lee of the wave crest. Over waves of small slope, with no separation, a *non-separated sheltering* leads to growth of the waves (Belcher & Hunt 1993; Miles 1993, 1996; van Duin 1996; Zou 1998). This mechanism complements the celebrated critical-layer mechanism of wave growth first analysed by Miles (1957). There have been studies of how turbulent stresses affect Miles' (1957) critical-layer mechanism (Miles 1993, 1996; Belcher, Hunt & Cohen 1998), but no definitive results have been found. These developments have been reviewed recently by Belcher & Hunt (1998).

Most of these recent studies have focused on waves that are strongly forced by the wind, so that  $c/u_*$  is small ( $c$  is the wave phase speed and  $u_*$  is the friction velocity in the wind). Belcher & Hunt (1993) called these slow waves. A practical reason for studying these slow waves is that they grow rapidly under the strong wind forcing. When the waves are slow the 'inner region', where the turbulent stresses have their strongest effect, is thin and the critical height,  $z_c$ , where the wind speed equals the wave speed is very close to the surface. Approximate analytical solutions then show that the critical layer does not have a strong dynamical effect on growth of slow waves (van Duin & Janssen 1992; Belcher & Hunt 1993; Miles 1996). As the wave speed increases, the critical height moves upwards away from the surface and eventually becomes comparable to the depth of the inner region. There is then a complicated interaction between the sheltering mechanism for wave growth and the critical-layer mechanism, the details of which have not been quantified (Belcher & Hunt 1998).

At faster wave speeds still, the critical height moves far above the wave surface: too far to have a significant dynamical effect on the flow. The dynamics of the air flow over these *fast waves* has not been studied before. These fast waves arise naturally in two important practical situations. First, fast waves arise as the sea state approaches 'full development' (Pierson & Moskowitz 1964), i.e. when waves at the peak in the spectrum have phase speeds approaching the synoptic wind speed. Nonlinear wave-wave interactions then transfer energy from the peak in the spectrum and generate waves of lower frequency, which travel faster than the wind. Secondly, when swell propagates away from a storm into areas of lighter winds, slow waves can become fast waves. Fast waves are also interesting for theoretical reasons. For fast waves the critical height either lies well above the wave surface, or does not exist at all if the wave travels faster than the wind. So effects of turbulent stresses are the only mechanism that can lead to asymmetry in the flow and thence energy exchange between the wind and waves. Even without detailed calculations we know that any interaction between fast waves and wind must be weak because it is well known that swell can propagate huge distances without being strongly affected by wind (e.g. Ursell 1954). Nevertheless, a comprehensive theory of wind-wave interaction should quantify the interaction, and should also show the circumstances when the interaction becomes stronger.

Here we develop an analytical model, formulated in §2, for linear changes to turbulent boundary layer flow over waves of small slope. We focus on waves that propagate in the same direction as the wind (although waves travelling against the wind can be treated with the model of Belcher & Hunt 1993). We show in §3 that the wave-induced air flow is usefully divided into 'inner' and 'outer' regions, where the turbulence responds to the wave differently and needs to be modelled differently. In §4 the momentum equations are scaled to determine the dominant balances, which

leads to the formal identification of the fast-wave limit. Approximate analytical solutions are then found for the wave-induced changes to the air flow in §5 based on the approximation that an ‘inner region’ is a thin ‘internal boundary layer’. The wave-induced pressure and stress do work at the surface which, as shown in §6, leads to growth of slow waves and decay of the fast waves. Finally conclusions are given in §7.

## 2. Formulation of the physical model

In the limit of vanishing waves, when the interface is flat and located at  $z = 0$ , air flows in the positive  $x$ -direction as the surface layer of a steady fully-developed neutrally-stable atmospheric boundary layer. The velocity profile in the air,  $\overline{U}_B(z)$ , is then logarithmic, namely  $\overline{U}_B = (u_*/\kappa) \ln(z/z_0)$ , where  $\kappa$  is the von Kármán constant (taken here to be 0.4), and  $z_0$  is the roughness parameter; the shear stress,  $\tau_B$ , is constant with height and equal to  $\rho_a u_*^2$ , where  $\rho_a$  is the density of the air and  $u_*$  is the friction velocity. We calculate the linear changes to this *basic flow* caused by a two-dimensional wave of small slope that travels along the air–water interface in the wind direction.

Perturbations to the basic flow are forced by two processes: (i) the undulating water surface and (ii) the non-zero velocity at the wave surface associated with the wave-induced water motions. Both processes scale on the wave slope and hence so do wave-induced perturbations to the basic flow. The wave slope is assumed here to be small, and we investigate linear changes to the basic flow. Then it is sufficient to consider sinusoidal waves described by  $z_s = \text{Re}\{ae^{ikx}\}$ , where  $a$  is the wave amplitude,  $k$  is the wavenumber, and the wave slope is  $ak \ll 1$ .

The roughness of the surface,  $z_0$ , represents the drag on the air flow of the small-scale waves riding along the primary sinusoidal wave. Hence we imply a scale separation between the primary wave, whose effect on the air flow we calculate explicitly, and the small-scale waves. Then  $kz_0$  is a small parameter of the model. The primary wave leads to a contribution to the drag on the air flow. Makin, Kudryatsev & Mastenbroek (1995) show how the total drag due to a wind sea with a broad spectrum of waves can be calculated by summing over the spectrum the drag due to a single sinusoidal wave. They show that this procedure yields a Charnock relation between the roughness and the friction velocity, namely  $z_0 \propto u_*^2/g$ . With this development in mind we prefer to keep  $kz_0$  a parameter of the present model rather than parameterising it using a Charnock relation, which some authors have advocated (see for example Komen *et al.* 1994, section II.2). In addition to  $kz_0 \ll 1$ , the parameters of the model are the wave slope,  $ak \ll 1$ , and the ratio of the wave speed to the wind speed,  $c/u_*$ ; their values are discussed in §4.2.

Calculations are performed in a reference frame moving with the wave crests, when at leading order the basic wind profile is simply displaced over the wave surface and can be written

$$U_B = \frac{u_*}{\kappa} \ln\{(z-s)/z_0\} - c, \quad (2.1)$$

where  $s$  is the vertical displacement of a mean streamline from its position in the unperturbed flow (see figure 1). Following Miles (1993) and Zou (1998) perturbations to the air flow induced by the travelling wave are analysed in terms of  $s(\xi, \eta)$ , where  $\eta$  labels the streamlines in the basic state, so that the streamfunction,  $\psi$ , is given by  $\psi = \int U_B(\eta) d\eta$ . The analysis is then performed in a streamline coordinate system,  $(\xi, \eta)$ , defined by

$$x = \xi, \quad z = \eta + s(\xi, \eta).$$

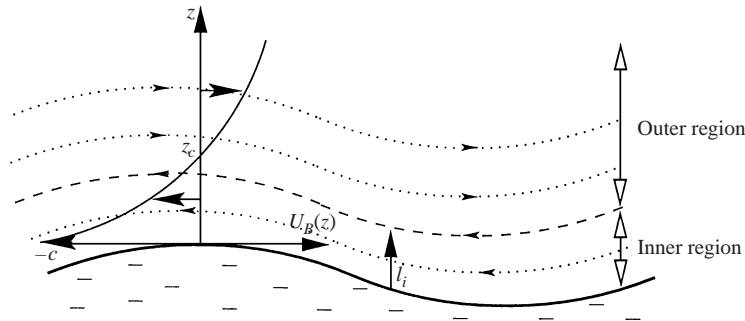


FIGURE 1. Schematic of the flow geometry.

The horizontal and vertical velocities over the wave,  $u$  and  $v$ , written in terms of this streamline coordinate system are

$$u = U_B + \tilde{u} = \frac{U_B(\eta)}{1 + \partial s / \partial \eta} \sim U_B(1 - \partial s / \partial \eta), \quad (2.2)$$

$$w = \tilde{w} = \frac{U_B(\eta) \partial s / \partial \xi}{1 + \partial s / \partial \eta} \sim U_B \partial s / \partial \xi, \quad (2.3)$$

which automatically satisfy continuity, and where the approximate forms are for waves of small slope. Upper-case letters with subscripts  $B$  denote variables associated with the basic flow, and an overbar denotes basic-state variables measured in the laboratory frame, otherwise the reference frame moves with the wave crests. The symbols  $\tilde{u}$  and  $\tilde{w}$  denote the wave-induced perturbations to the horizontal and vertical velocity.

If the ensemble-averaged Navier–Stokes equations are transformed into the streamline coordinate system and then linearised for small perturbations, then the horizontal and vertical momentum equations become

$$U_B \frac{\partial \tilde{u}}{\partial \xi} = -\frac{\partial \tilde{p}}{\partial \xi} + \frac{\partial \tilde{\tau}}{\partial \eta}, \quad (2.4)$$

$$U_B \frac{\partial \tilde{w}}{\partial \xi} = -\frac{\partial \tilde{p}}{\partial \eta} + \frac{\partial \tilde{\tau}}{\partial \xi}, \quad (2.5)$$

which show the power of the streamline coordinate system, namely that the advective rates of change are only in the  $\xi$ -direction, i.e. along the streamlines. Here,  $\tilde{\tau}$  is the wave-induced turbulent shear stress; the wave-induced normal turbulent stresses are neglected in the analysis here because their effects are smaller than the dominant terms calculated (Townsend 1972).

The boundary condition on  $u$  at the wave surface is the no-slip condition, so that the wave-induced flow must match the tangential velocity associated with the orbital motions in the water,  $\tilde{u}_s$ . The boundary condition on  $w$  arises from local continuity and ensures that the surface is a streamline, i.e.  $w(z_0) = Dz_s/Dt$ . Hence

$$u = -c + \tilde{u}_s, \quad w = -c dz_s/d\xi \quad \text{on } \eta = z_0. \quad (2.6)$$

This shows a second advantage of the streamline coordinates, namely that boundary conditions can be applied actually at the boundary, rather than being linearized onto a horizontal surface. For linear irrotational water waves on deep water, and neglecting any small drift current in the water,  $\tilde{u}_s = \text{Re} \{ akc e^{ik\xi} \}$ . In addition, the wave-induced

flow decays to zero far above the air–water interface, i.e.

$$\tilde{u}, \tilde{w} \rightarrow 0 \quad \text{as} \quad k\eta \rightarrow \infty. \quad (2.7)$$

Equations and boundary conditions have now been formulated for describing linear changes to the streamline displacement  $h(\eta)$  forced by a travelling wave. The formulation is completed by specifying a model for the wave-induced perturbations to the turbulent shear stress,  $\tilde{\tau}$ . This important issue is discussed next.

### 3. Inner and outer regions

Following previous studies of turbulent boundary layer flow over hills (Jackson & Hunt 1975; Britter, Hunt & Richards 1981), and over waves (Townsend 1972, 1980; Belcher & Hunt 1993), it is helpful to divide the flow over the waves into inner and outer regions, where different physical processes dominate (refer to figure 1). As reviewed recently by Belcher & Hunt (1998), the effects of a travelling wave on turbulence in the air flow can be understood by examining the ratio of an advection time scale,  $T_A$ , to an eddy decorrelation time scale,  $T_L$ . These ideas are briefly recounted here, and following Cohen (1997) some new thoughts are given on how they apply to fast-moving waves.

The advection time scale,  $T_A$ , is a time scale for turbulent eddies to be distorted as they are advected by the mean flow over a wavelength. Hence the appropriate advection speed is relative to the wave, i.e.  $U_B(\eta) = \bar{U}_B - c$ . The main new idea required to apply this scaling argument to fast waves is the recognition that above the critical height the mean-flow advection is in the positive  $x$ -axis direction, but below the critical height it is in the negative  $x$ -direction. For the purpose of scaling it is the magnitude, and not the sign, of  $T_A$  that is important, and so to keep the definition of  $T_A$  positive, the modulus of  $U_B(\eta)$  is used, hence

$$T_A = k^{-1}/|U_B(\eta)|. \quad (3.1)$$

This definition of the advection time scale is then appropriate for the whole range of wind and waves speeds, including fast waves. The eddy-decorrelation time scale,  $T_L$ , characterizes the time it takes for eddies to decorrelate and interact with one another, and so it is also the time scale for turbulence to come into equilibrium with the surrounding mean-flow velocity gradient. The strong density jump at the air–sea interface constrains the turbulence as a solid wall would (Lombardi, De Angelis & Bannerjee 1996) and so an estimate for  $T_L$  follows the estimate in a wall boundary layer, namely

$$T_L = k\eta/u_*. \quad (3.2)$$

The ratio of these time scales gives a measure of how far the turbulence is from a local equilibrium. When  $T_L \ll T_A$  turbulent eddies decorrelate many times before being advected over the wave. Hence these eddies approach local equilibrium with local production of turbulent kinetic energy balancing dissipation. The mixing-length model can then be used to relate the wave-induced Reynolds stress to the local wave-induced mean-velocity gradient (Townsend 1961); hence, on using the linearized form of (2.2),

$$\tilde{\tau}_{ml} = 2\kappa u_* \eta \frac{\partial \tilde{u}}{\partial \eta} = -2\kappa u_* \eta \frac{\partial}{\partial \eta} \left( U_B(\eta) \frac{\partial s}{\partial \eta} \right). \quad (3.3)$$

In contrast, when  $T_L \gg T_A$ , the turbulent eddies are carried over the wave by the mean flow more rapidly than they can turn over and interact nonlinearly. The eddies

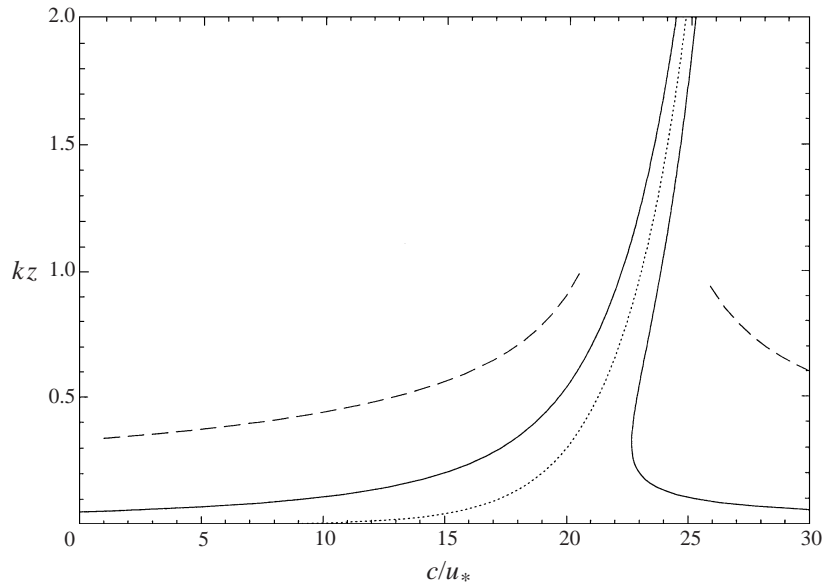


FIGURE 2. Variation of depth of the inner region (solid line), critical height (dotted line) and middle layer height (dashed line);  $kz_0 = 10^{-4}$ .

are then distorted primarily by the mean straining by the wave-induced air flow, and can be described using rapid distortion theory (Britter *et al.* 1981).

These two limiting behaviours both occur in the flow over a wave because  $T_L$  increases and  $T_A$  decreases with height above the wave surface. They are equal,  $T_A = T_L$ , at heights  $\eta = l_i$ , defined implicitly by

$$kl_i |\ln(l_i/z_0) - \kappa c/u_*| = 2\kappa^2. \quad (3.4)$$

The value of the order-one constant on the right is chosen to be consistent with the scaling of the mean momentum equation, described in §4.2.

Figure 2 shows the variation of  $l_i$  with  $c/u_*$ , when  $kz_0 = 10^{-4}$  (a typical oceanic value). As shown by Belcher & Hunt (1993), for slow waves there is just one value of  $l_i$  and the air flow can be divided into two regions: an 'inner' equilibrium region,  $\eta < l_i$ , where  $T_L < T_A$ , and an 'outer' rapid-distortion region,  $\eta > l_i$ , where  $T_A < T_L$ . For these small values of  $c/u_*$  the critical height,  $z_c$ , lies well within the inner region.

When negative advection below the critical height is correctly accounted for by including the modulus signs in (3.1) there are three solutions to (3.4) when  $c/u_*$  is larger than  $(c/u_*)_b = \{\ln(2\kappa^2/kz_0) + 1\}/\kappa$ . The lowest solution,  $l_i$ , defines a region close to the surface,  $\eta < l_i$ , where  $T_L < T_A$ , which is therefore an equilibrium region that is called here the inner region. Above this inner region,  $T_A < T_L$  and the turbulence is distorted rapidly, except for a thin layer between the other two solutions to (3.4) which lie either side of the critical height (figure 2). Hence the flow can be considered to have an 'outer' rapid-distortion region above the inner region. Near the critical height the mean-flow advection is small and so  $T_L < T_A$ , which suggests that the eddies reach a local equilibrium. But as noted by Phillips (1977, p. 121) turbulent fluctuations transport eddies vertically across this critical layer in a time that is too short for a local equilibrium to become established and so in this intermediate regime, when the critical height is neither very far from nor very close to the interface (i.e.  $kz_c = O(1)$ ), a new time scale associated with this turbulent transport would need to be analysed.

In the fast wind-wave parameter regime analysed here it is not necessary to analyse this region around the critical layer because it lies too far from the interface to affect the dynamics (see §4). Also shown on figure 2 is the height of the ‘middle layer’  $kz = (\delta/\kappa)^{1/2}$  where, as explained in §5.6, the pressure perturbation is determined.

Here, following Harris, Belcher & Street (1996), van Duin (1996) and Cohen (1997), the wave-induced Reynolds shear stress is parameterized so that it interpolates between the mixing-length model (3.3) in the inner region and zero in the outer region. Specifically we use

$$\tilde{\tau} = \tilde{\tau}_{ml} \exp\{-k\eta/\delta^n\}, \quad (3.5)$$

where  $\tilde{\tau}_{ml}$  is the stress from the mixing-length model (3.3) and  $\delta = u_*/|U_1|$ . The parameter  $n$  is chosen to lie between 0 and 1 so that the exponential decay occurs in the overlap between the inner and outer regions. This model works equally well for both fast and slow waves because, as explained above, inner and outer regions can be defined in both regimes. Hence the mixing-length model is appropriate in the inner region for both regimes, but must be damped to zero in the outer region of both regimes.

The model (3.5) parameterizes explicitly neither the advection of stress that becomes important around  $\eta \sim l_i$ , nor the rapid-distortion processes in the outer region; previous experience suggests that it is sufficient to calculate the wave-induced flow and wave growth rate (see e.g. Belcher & Hunt 1998 or the comments given in §6 following comparisons with other studies).

An elegant alternative to this explicit damping has been proposed by Townsend (1972), who developed a transport equation for the wave-induced stress that has been used in analytical studies of boundary layer flow over waves and hills by Miles (1996) and Zou (1998). This equation tends to the mixing-length model for the stress towards the surface, and gives a wave-induced stress of the correct magnitude in the outer region. The equation does not, however, model explicitly the rapid response of the turbulence in the outer region (Townsend 1980). The simpler approach (3.5) is preferred here as it simplifies the analysis and also to illustrate that it contains the essential dynamical elements.

#### 4. Scale analysis and definition of fast waves

We have developed the idea of dividing the flow into inner and outer regions based on the behaviour of the turbulence in the distorted boundary layer. Now consider how the turbulent stresses affect the mean flow in the inner and outer regions. Hence in §4.1, below, the dominant dynamical balances in the horizontal momentum equation (2.4) are determined using scaling estimates. This scaling leads to identification of a parameter,  $\delta$ ; when  $\delta$  is small, solutions for the mean flow can be found using asymptotic methods. Hence, in §4.2 we determine the range of wind and wave speeds required for  $\delta$  to be small.

##### 4.1. Dominant balances in the inner and outer regions

The dominant balance in the streamwise momentum equation (2.4) changes through the depth of the wave-induced flow, partly because different estimates are needed for the shear stress in the different regions of the flow, and partly because the advection speed varies with depth. In the rapid-distortion region, exact rapid-distortion calculations (Britter *et al.* 1981; Belcher *et al.* 1993) show that

$$\tilde{\tau} = O(u_*^2 \tilde{u}/U_B) = O(aku_*^2). \quad (4.1)$$

These exact calculations show clearly that the same scaling applies to the outer region in both the slow and fast waves. In the local-equilibrium region the mixing-length model (3.3) scales as

$$\tilde{\tau} = -2\kappa u_* \eta \frac{\partial}{\partial \eta} \left( U_B \frac{\partial s}{\partial \eta} \right) = O \left( \kappa u_* \eta \frac{1}{\eta} U_B \frac{a}{\eta} \right). \quad (4.2)$$

Then in the outer region, where there is rapid distortion and  $k\eta = O(1)$ , the ratio of terms in the streamwise momentum equation (2.4) is

$$\left| \frac{\text{stress gradient term}}{\text{advection term}} \right| = \left| \frac{\partial \tilde{\tau} / \partial \eta}{U_B \partial \tilde{u} / \partial \xi} \right| = O \left( \frac{a \kappa u_*^2}{a \kappa U_1^2} \right) = O(\delta^2), \quad (4.3)$$

where  $U_1 = U_B(1/k)$  and  $\delta = u_* / |U_1|$ . Thus if  $\delta \ll 1$  the perturbation Reynolds stress leads to only very small changes to the mean flow in the region of rapid distortion.

In the inner region, adjacent to the wave surface, where  $\eta = O(l_i)$  and the turbulence tends to local equilibrium, and using (2.2) to estimate  $\tilde{u}$ , shows that

$$\left| \frac{\text{stress gradient term}}{\text{advection term}} \right| \sim \left| \frac{\{u_* l_i (U_B(l_i) a / l_i) / l_i\} / l_i}{U_B(l_i) i \kappa a U_B(l_i) / l_i} \right| \sim \frac{u_*}{|U_B(l_i)|} \frac{1}{k l_i} = O(1) \quad (4.4)$$

on using (3.4), the definition of  $k l_i$ . Hence mean-flow advection balances the perturbation stress gradient in the inner region.

Now if the relative thickness of the inner region,  $k l_i$ , is small then the inner region can be analysed as a thin internal boundary layer and it is easy to show that  $k l_i = O(\delta)$  when  $\delta \ll 1$  (see Cohen 1997). Therefore internal-boundary-layer methods may be used to analyse the inner region when  $\delta \ll 1$ . Next the wind-wave parameters that give  $\delta \ll 1$  are determined.

#### 4.2. Definition of slow and fast waves

With the present model formulation, there are two independent parameters that specify the problem: the relative roughness of the wave,  $k z_0$ , and the relative wave speed,  $c/u_*$ . We now determine how the relative values of these parameters determine the wind-wave regime. Hence we consider the limit  $k z_0 \rightarrow 0$  and determine the range of values of  $c/u_*$  required for slow and fast waves.

The slow and fast wind-wave regimes are distinguished by small values of the parameter  $\delta$ , which can be written in terms of the relative height of the critical level,  $k z_c$ :

$$\delta = u_* / |U_1| = \kappa / |\ln(1/k z_0) - \kappa c / u_*| = \kappa / |\ln(k z_c)|. \quad (4.5)$$

Hence  $\delta$  is small when either  $k z_c$  is small, so that the critical height lies close to the surface, or when  $k z_c$  is large, so that the critical height lies well above the surface.

First, the limit of *slow waves*, when  $k z_c$  is small and lies close to the surface, requires

$$k z_c = k z_0 e^{\kappa c / u_*} \ll 1. \quad (4.6)$$

Belcher & Hunt (1993) show that this condition is equivalent to  $\kappa c / u_* = O(1)$  as  $\delta \rightarrow 0$ , hence slow waves.

Secondly, in the limit of *fast waves*, when  $k z_c$  is large, it is helpful to suppose that  $k z_c = (1/k z_0)^p$ , so that  $k z_c \rightarrow \infty$  as  $k z_0 \rightarrow 0$ . In this limit the critical height is far from the wave surface, so the Miles (1957) critical-layer mechanism of wave growth must be small and therefore can be neglected here. This relation between  $k z_c$  and  $k z_0$  means that

$$\delta = \frac{\kappa}{|\log(k z_c)|} = \frac{\kappa}{p \log(1/k z_0)}. \quad (4.7)$$



Combining the definition  $kz_c = kz_0 e^{kc/u_*}$  with  $kz_c = (1/kz_0)^p$  shows that the relative wave speed is given by

$$\kappa c/u_* = (p + 1) \ln(1/kz_0). \tag{4.8}$$

Therefore (4.7) and (4.8) combine to give

$$\frac{\delta c}{u_*} = \frac{1 + p}{p} = C \quad \text{which is chosen to be fixed and } O(1) \text{ as } \delta \rightarrow 0. \tag{4.9}$$

We define this relationship between the two basic parameters,  $\delta = u_*/|U_1|$  and  $c/u_*$ , namely the limit  $\delta \rightarrow 0$  with  $\delta c/u_*$  fixed and  $O(1)$ , to be the formal limit for fast waves.

In practice the wind-wave regime is easily calculated by computing the value of  $\delta/\kappa$  (which the analysis of §5 shows to be the relevant parameter). Hence the wind waves are defined to be slow or fast when  $\delta/\kappa < 1$ . Then, accounting for the modulus sign in the definition of  $\delta$ , slow waves are defined by  $c/u_* < \{\ln(1/kz_0) - 1\}/\kappa$  and fast waves by  $c/u_* > \{\ln(1/kz_0) + 1\}/\kappa$ . When  $kz_0 = 10^{-4}$  this classification yields slow waves when  $0 < c/u_* < 20$  and fast waves when  $25 < c/u_*$ .

### 5. Asymptotic solution for air flow over fast waves

A single equation for the streamline displacement is obtained by eliminating pressure between the nonlinear counterparts of (2.4) and (2.5) and then substituting for  $\tilde{u}$  and  $\tilde{w}$  using (2.2) and (2.3). The result is linearized for small perturbations and the streamline displacement is written  $s = \text{Re}\{h e^{ikx}\}$ , where  $h$  is a complex amplitude. Similarly other wave-induced variables are written as complex amplitudes, e.g.  $\tilde{u} = \text{Re}\{\hat{u} e^{ikx}\}$ . This procedure shows that the linear displacement of the streamline,  $h$ , is governed by

$$-\frac{\partial}{\partial \eta} \left( U_B^2 \frac{\partial h}{\partial \eta} \right) + k^2 U_B^2 h = -i \frac{1}{k} \frac{\partial^2 \hat{\tau}}{\partial \eta^2} - ik \hat{\tau} \tag{5.1}$$

(cf. Miles 1993; Zou 1998), which is the Rayleigh equation transformed into the streamline coordinate system with forcing from the wave-induced turbulent stress, which is modelled according to (3.5). The boundary conditions (2.6) and (2.7) are transformed into boundary conditions on the streamline displacement,  $h(\eta)$ , using (2.2) and (2.3), which gives

$$h = a, \quad \frac{\partial h}{\partial \eta} = ak \quad \text{on } \eta = z_0, \quad \text{and } h, \quad \frac{\partial h}{\partial \eta} \rightarrow 0 \quad \text{as } \eta \rightarrow \infty. \tag{5.2}$$

These equations are now solved for fast waves using formal asymptotic expansions in each of the regions.

A dimensionless basic velocity profile is defined to be

$$V(\eta) = U_B(\eta)/U_1 \quad \text{where } U_1 = U_B(1/k). \tag{5.3}$$

Then, since  $U_1 < 0$  for fast waves, in the range  $z_0 < \eta < 1/k$  the dimensionless velocity is in the range  $0 < V(\eta) < 1$ . Then  $\delta = u_*/|U_1| = -u_*/U_1$  for fast waves. Throughout the analysis the amplitude of the streamfunction displacement,  $h$ , is normalized on wave amplitude,  $a$ , and is distinguished in the different layers by a subscript, e.g.  $h_i$  for the inner region.

## 5.1. Outer region

The outer region is split into two layers: the *upper layer* where the effect of the perturbation shear stress is exponentially small; and, nearer the surface, the *transition layer*, which resolves the decay of the eddy viscosity and there are weak  $O(\delta)$  interactions between the advection of the mean flow and the perturbation shear stress.

## 5.1.1. Upper layer

In the upper layer the height is made dimensionless on  $1/k$  so that  $\eta_1 = k\eta$ , then (5.1) reduces to

$$\frac{\partial^2 h_1}{\partial \eta_1^2} - h_1 = -2 \frac{V'}{V} \frac{\partial h_1}{\partial \eta_1} + O(\delta \exp\{-\eta_1/\delta^n\}). \quad (5.4)$$

The exponentially small correction on the right is from the Reynolds stress gradients, which have been forced here to be exponentially small through the damping in the model for  $\tilde{\tau}$  in (3.5). Solutions to (5.4) can be found based on the approximation that the shear is weak. For a logarithmic basic flow

$$V'/V = -\delta/\kappa V \eta_1, \quad (5.5)$$

which is small and  $O(\delta)$  in the upper layer where  $\eta_1 = O(1)$ . Hence, the dynamics are governed by a Rayleigh equation with weak shear, and solutions can be found using the methods developed by Lighthill (1957), namely by expanding  $h_1$  in powers of  $\delta$ :

$$h_1 = h_1^{(0)} + \delta h_1^{(1)} + \delta^2 h_1^{(2)} + O(\delta^3). \quad (5.6)$$

We find the following iterative solution:

$$\left. \begin{aligned} h_1^{(0)} &= H_0 e^{-\eta_1}, \\ h_1^{(i)} &= H_i e^{-\eta_1} - e^{\eta_1} \int^{\eta_1} \frac{V'}{V} \frac{dh^{(i-1)}}{dy} e^{-y} dy + e^{-\eta_1} \int^{\eta_1} \frac{V'}{V} \frac{dh^{(i-1)}}{dy} e^y dy, \end{aligned} \right\} \quad (5.7)$$

where  $H_i$  are unknown constants determined by matching with solutions in the lower layers. Explicit forms of the solution up to  $O(\delta^2)$  are given by Cohen (1997).

Towards the surface, as  $\eta_1$  decreases, the upper-layer solution becomes invalid because both the shear term and the gradient of the perturbation shear stress in (5.1) become important. Hence the *transition layer* needs to be analysed.

## 5.1.2. Transition layer

In the transition layer the vertical coordinate is  $\eta_1 = \delta^n \eta_t$ , with  $\eta_t = O(1)$  so that the exponential decay of the stress model is resolved. Then (5.1) reduces to

$$\frac{\partial}{\partial \eta_t} \left( V^2 \frac{\partial h_t}{\partial \eta_t} \right) = \delta^{2n} V^2 h_t + i \delta^{1-n} \frac{\partial^2 \hat{\tau}_t}{\partial \eta_t^2}, \quad (5.8)$$

where the rescaled dimensionless shear stress,  $\hat{\tau}_t$ , is

$$\hat{\tau}_t = 2\kappa \eta_t \frac{\partial}{\partial \eta_t} \left( V \frac{\partial h_t}{\partial \eta_t} \right) e^{-\eta_t}. \quad (5.9)$$

Hence, the dynamics are controlled by the Rayleigh equation in the long-wave limit, with small corrections for the finite wavelength (the first term on the right of (5.8)), and for small stress gradients (the second term on the right of (5.8)).

Solutions are found by expanding  $h_t$  in powers of  $\delta$ :

$$\begin{aligned}
 h_t &= h_t^{(0)} + \delta^n h_t^{(1)} + \delta^{2n} h_t^{(2)} + \dots \\
 &\quad + \delta h_t^{(3)} + \delta^{1+n} h_t^{(4)} + \dots \\
 &\quad + \delta^2 h_t^{(5)} + \dots,
 \end{aligned}
 \tag{5.10}$$

where the neglected terms of  $O(\delta^{3n})$ ,  $O(\delta^{1+2n})$  and  $O(\delta^{1+n})$  are not required when matching with the upper and shear stress layers. Substitution of this expansion into (5.8) leads to a sequence of differential equations that are solved at each order in  $\delta$  to yield

$$\left. \begin{aligned}
 h_t^{(0)} &= T_0, \\
 h_t^{(1)} &= T_1 \int^{\eta_t} \frac{1}{V^2} dx + T_2, \\
 h_t^{(2)} &= T_0 \int^{\eta_t} \frac{1}{V^2} \int^x V^2 dy dx + T_3 \int^{\eta_t} \frac{1}{V^2} dx + T_4, \\
 h_t^{(3)} &= -2\kappa i T_1 \int^{\eta_t} \frac{1}{V^2} \frac{\partial}{\partial x} \left( \frac{e^{-x}}{V^2} x \frac{\partial V}{\partial x} \right) dx + T_5 \int^{\eta_t} \frac{1}{V^2} dx + T_6, \\
 h_t^{(4)} &= 2\kappa i T_0 \int^{\eta_t} \frac{1}{V^2} \frac{\partial}{\partial x} \left\{ x e^{-x} \frac{\partial}{\partial x} \left( \frac{1}{V} \int^x V^2 dy \right) \right\} dx \\
 &\quad - 2\kappa i T_3 \int^{\eta_t} \frac{1}{V^2} \frac{\partial}{\partial x} \left( \frac{e^{-x}}{V^2} x \frac{\partial V}{\partial x} \right) dx + T_7 \int^{\eta_t} \frac{1}{V^2} dx + T_8, \\
 h_t^{(5)} &= T_9 - i T_1 \frac{2}{V^4} e^{-\eta_t} + \text{other terms.}
 \end{aligned} \right\}
 \tag{5.11}$$

The ‘other terms’ in  $h_t^{(5)}$  are not required to match to  $O(\delta^2)$  with the solutions in the upper layer and inner region.

As shown in detail in Cohen (1997), matching the transition-layer and upper-layer solutions, using the intermediate variable  $\eta_1 = \delta^\alpha \eta_{ut}$  where  $0 < \alpha < n$ , relates the  $T_n$  to the  $H_n$ :

$$\left. \begin{aligned}
 T_0 = H_0, \quad T_1 = -H_0, \quad T_2 = 0, \quad T_3 = 0, \quad T_4 = 0, \\
 T_5 = 0, \quad T_6 = H_1, \quad T_7 = -H_1, \quad T_8 = 0, \quad T_9 = H_2.
 \end{aligned} \right\}
 \tag{5.12}$$

### 5.2. Fast waves and very fast waves

There are two subranges of fast waves, namely *fast* and *very fast waves*, that correspond mathematically to whether or not  $z_0/l_i$  is small. To explain this difference recall that, as shown in §4.1, across the bulk of the inner region, advection balances the perturbation stress gradient. But very close to the wave surface, where  $\eta = O(z_0)$  and  $U_B(z_0) = -c$

$$\frac{\text{advection term}}{\text{stress gradient term}} = O \left( \frac{k U_B^2(z_0) a / z_0^2}{u_* U_B(z_0) a / z_0^3} \right) = O \left( \frac{k z_0}{u_* / c} \right).
 \tag{5.13}$$

Hence for this balance between advection and stress gradient to persist right down to the air–water interface requires  $k z_0 c / u_* = O(1)$  as  $\delta \rightarrow 0$ , which requires very fast waves speeds: much faster than required by the limit  $\delta c / u_* = O(1)$  established in §4.2 for fast waves. Hence there are two subregimes of fast waves. Wind-wave

systems that satisfy  $kz_0c/u_* = O(1)$  are termed here *very fast waves* and are treated separately in § 5.5. Solutions for very fast waves are denoted with superscript (*vf*). In the more typical *fast-wave subregime*, when  $\delta c/u_* = O(1)$ , the ratio in (5.13) becomes  $kz_0c/u_* \rightarrow 0$  as  $kz_0 \rightarrow 0$ . So that as the surface is approached the advection becomes too weak to balance the gradient of the perturbation shear stress. In this case an *inner surface layer* must be analysed where the shear stress gradient is zero to leading order (cf. the analysis of Sykes 1980 of flow over hills). The remainder of the inner region, where advection balances stress gradient, is called here the *inner shear stress layer*. Solutions in the fast-wave regime are denoted with a supscript (*f*).

### 5.3. Inner shear stress layer for fast waves

Within the inner region, the vertical coordinate is  $\eta = l_i \eta_i$ , with  $\eta_i = O(1)$ . Furthermore, the mean velocity written in terms of this inner region variable is

$$V(\eta_i) = V_i - \frac{\delta}{\kappa} \ln \eta_i, \quad (5.14)$$

where  $V_i = U_B(l_i)/U_1$  is  $O(1)$  as  $\delta \rightarrow 0$  (Cohen 1997). The governing equation for  $h_i$  in inner region then becomes

$$\begin{aligned} -i \frac{\partial^2}{\partial \eta_i^2} \left( \eta_i \frac{\partial^2 h_i}{\partial \eta_i^2} \right) + \frac{\partial^2 h_i}{\partial \eta_i^2} = \delta \frac{1}{\kappa V_i} \left[ \frac{2}{\eta_i} \frac{\partial h_i}{\partial \eta_i} + 2 \ln \eta_i \frac{\partial^2 h_i}{\partial \eta_i^2} - i \frac{\partial^2}{\partial \eta_i^2} \left\{ \eta_i \frac{\partial}{\partial \eta_i} \left( \frac{\partial h_i}{\partial \eta_i} \ln \eta_i \right) \right\} \right] \\ + \delta^2 \left( \frac{2\kappa}{V_i} \right)^2 h_i + O \left( \delta^2 \frac{\partial^m h_i}{\partial \eta_i^m} \right) + O(\delta^3), \quad (5.15) \end{aligned}$$

where  $m \geq 1$  is an integer so that neglected terms at  $O(\delta^2)$  contain derivatives of  $h_i$ . For these terms to contribute to the  $O(\delta^2)$  solution calculated here the derivatives of the  $O(1)$  solution would need to be non-zero; however it will be shown later that  $h_i$  is constant at  $O(1)$ . There are four linearly-independent solutions for  $h_i$  to the leading-order homogeneous equation, namely a constant,  $\eta_i$ ,  $K_0^*(X)$  and  $I_0^*(X)$ , where  $K_0^*$  and  $I_0^*$  are the complex conjugates of the zeroth-order modified Bessel functions of the second kind (Abramowitz & Stegun 1972) and  $X = 2(i\eta_i)^{1/2}$ . But  $I_0^*$  grows exponentially at large heights and so is rejected as not being physical.

The amplitude of the streamline displacement,  $h_i$ , is expanded in powers of  $\delta$

$$h_i^{(f)} = h_i^{(0)} + \delta h_i^{(1)} + \delta^2 h_i^{(2)} + O(\delta^3), \quad (5.16)$$

and equation (5.15) is then solved iteratively to give

$$\begin{aligned} h_i^{(f)} = I_0^{(f)} + \delta \left( I_1^{(f)} \eta_i + I_2^{(f)} \right) + \delta^2 \left\{ I_3^{(f)} \eta_i \frac{\partial K_0^*}{\partial \eta_i} + I_4^{(f)} \eta_i + I_5^{(f)} + I_0^{(f)} \left( \frac{2\kappa}{V_i} \right)^2 \frac{\eta_i^2}{2} \right. \\ \left. + \frac{2}{\kappa V_i} I_1^{(f)} \eta_i (\ln \eta_i - 1) \right\} + O(\delta^3), \quad (5.17) \end{aligned}$$

where, for brevity, the homogeneous solutions are included only when their coefficients,  $I_n$ ,  $n = 1 \dots 5$ , eventually turn out to be non-zero when they are obtained by matching with the adjacent layers.

Cohen (1997) shows that matching these solutions with the transition layer, using the intermediate variable  $\eta_1 = \delta^\beta \eta_{ii}$  where  $n < \beta < 1$ , gives

$$I_0^{(f)} = T_0, \quad I_1^{(f)} = -\frac{2\kappa}{V_i^3} T_0, \quad I_2^{(f)} = T_6, \quad I_4^{(f)} = i \frac{4\kappa^2}{V_i^2} T_0 - \frac{2\kappa}{V_i^3} T_6, \quad I_5^{(f)} = T_9. \quad (5.18)$$

This solution in the shear stress layer ceases to be asymptotic in the limit of small  $\eta_i$  because the gradient of the fourth term in (5.17),  $\delta^2 I_3^{(f)} \eta_i \partial K_0^* / \partial \eta_i$ , diverges logarithmically as  $\eta_i \rightarrow 0$ . Therefore it is necessary to analyse an inner surface layer where  $\eta \sim O(z_0)$ . Between the inner shear stress layer and inner surface layer, it is simpler to match the wave-induced streamwise velocity, calculated from (5.17) using (2.2), which is given by

$$\hat{u} \sim -ak \frac{U_i^2}{2\kappa U_1} \left[ I_1^{(f)} + \delta \left\{ -iI_3^{(f)} K_0^* + I_0^{(f)} \frac{4\kappa^2}{V_i^2} \eta_i + I_4^{(f)} + \frac{I_1^{(f)}}{\kappa V_i} \ln \eta_i \right\} + O(\delta^2) \right]. \quad (5.19)$$

This expression, in the limit of small  $\eta_i$ , when  $K_0^* \rightarrow -\frac{1}{2} \ln \eta_i$ , is matched with the solution in the inner surface layer, which is derived next.

5.4. Inner surface layer for fast waves

The vertical coordinate in the inner surface layer is made dimensionless on  $z_0$ , so that  $\eta = z_0 \eta_0$  with  $\eta_0 = O(1)$ . Then equation (5.1), which governs the air flow perturbations, becomes

$$\frac{\partial^2 \hat{\tau}}{\partial \eta_0^2} = -\frac{kz_0}{\delta} \frac{i}{2\kappa^2} \frac{\partial}{\partial \eta_0} \left\{ (\ln \eta_0 - \kappa c / u_*)^2 \frac{\partial h_0}{\partial \eta_0} \right\} + O\{(kz_0)^2\}, \quad (5.20)$$

which just states that, at leading order in  $kz_0/\delta$ , the stress is constant across the inner surface layer (cf. Sykes 1980; Zou 1998). The terms of  $O(kz_0/\delta)$  are exponentially small compared with powers of  $\delta$  and so are negligible here. Hence the wave-induced stress and streamwise velocity in the inner surface layer are

$$\hat{\tau} \sim ak u_*^2 \left\{ S_0^{(f)} + O(kz_0/\delta^2) \right\}, \quad (5.21)$$

$$\hat{u} \sim ak \left\{ c + \frac{1}{2} S_0^{(f)} \frac{u_*}{\kappa} \ln \eta_0 + O(u_* kz_0) \right\}. \quad (5.22)$$

Matching this solution for  $\hat{u}$  with the solution in the inner shear stress layer (5.19) is delicate and needs to be done rigorously by rewriting each solution in terms of an intermediate variable  $\eta_{i0}$ , defined by  $\eta = (z_0/l_i)^{\alpha} l_i \eta_{i0}$ . The solutions are then matched in the limit  $z_0/l_i \rightarrow 0$  with  $\eta_{i0} = O(1)$ . This procedure determines the remaining unknown constants to be

$$\left. \begin{aligned} I_0^{(f)} = 1, \quad I_2^{(f)} = 0, \quad I_3^{(f)} = 2I_5^{(f)} = -2i \left( \frac{S_0^{(f)}}{V_i^2} + \frac{2}{V_i^4} \right), \\ S_0^{(f)} = \frac{2}{V_i^2} \left( 1 - \frac{c}{U_i} \right) - 2 \frac{c}{U_i}. \end{aligned} \right\} \quad (5.23)$$

5.5. Inner region for very fast waves

In the very fast sub-regime the inner region is governed by the same equation as for the inner shear stress layer of the fast sub-regime, namely (5.15). The difference is that there is no inner surface layer and boundary conditions at the wave surface are applied directly to the solution to this equation. It is found that the Bessel function then has a non-zero coefficient at  $O(\delta)$  rather than  $O(\delta^2)$ , and so the solution is

$$h_i^{(vf)} = I_0^{(vf)} + \delta \left( I_1^{(vf)} \eta_i + I_2^{(vf)} + I_3^{(vf)} \eta_i \frac{\partial K_0^*}{\partial \eta_i} \right) + O(\delta^2). \quad (5.24)$$

Matching with the transition layer gives

$$I_0^{(vf)} = T_0, \quad I_1^{(vf)} = -\frac{2\kappa}{V_i^3} T_0, \quad I_2^{(vf)} = T_6^{(vf)}. \quad (5.25)$$

Application of the boundary conditions at the wave surface then yields

$$\left. \begin{aligned} I_0^{(vf)} = 1, \quad I_2^{(vf)} = -\frac{z_0}{l_i} \frac{2\kappa}{V_i} \left\{ i \left( \frac{1}{V_i^2} + 1 \right) \left( \frac{\partial K_{0s}^*}{\partial \eta_i} \right) \left( \frac{1}{K_{0s}^*} \right) - \frac{1}{V_i^2} \right\}, \\ I_3^{(vf)} = i \frac{2\kappa}{V_i} \left( \frac{1}{V_i^2} + 1 \right) \left( \frac{1}{K_{0s}^*} \right), \end{aligned} \right\} \quad (5.26)$$

where  $K_{0s}^* = K_0^*(z_0/l_i)$ , and  $\partial K_{0s}^*/\partial \eta_i = \partial K_0^*/\partial \eta_i|_{\eta_i=z_0/l_i}$ . These solutions agree with the solutions for fast waves in the limit that  $z_0/l_i \rightarrow 0$ .

### 5.6. Determination of the surface pressure perturbation

The solutions found above for the streamline displacement,  $h$ , are now used to compute the asymmetric part of the wave-induced pressure through the boundary layer, and thence the asymmetric part of the surface pressure which contributes to growth of the waves. For a linear analysis of flow over a sinusoidal wave the wave-induced pressure can be represented as  $\tilde{p}(\xi, \eta) = \text{Re}\{\hat{p}(\eta) e^{ik\xi}\}$ , where  $\hat{p}(\eta)$  is a complex amplitude. The asymmetric part of the pressure is then contained in  $\text{Im}\{\hat{p}\}$ . This pressure contribution is calculated here from the vertical momentum equation, (2.5), so that, on using (2.3) to relate  $\tilde{w}$  to  $s$ , the imaginary part of the pressure amplitude is obtained from

$$\text{Im} \left\{ \frac{\partial \hat{p}}{\partial \eta} \right\} = k^2 \text{Im}\{U_B^2 h\} + k \text{Re}\{\hat{\tau}\}. \quad (5.27)$$

The surface pressure is obtained by integrating (5.27) through each of the layers using solutions in each of the layers for  $h$ , which have been calculated above, and for  $\hat{\tau}$ , which have been calculated from the solutions for  $h$  and are listed in Appendix A.

In the inner surface layer, the solution (A 12) shows that  $\text{Im}\{h\} = o(a\delta kz_0)$  and (A 13) shows that  $\text{Re}\{\hat{\tau}\} = O(aku_*^2)$ . But the inner surface layer is so thin that the pressure varies there by only an exponentially small amount, so that through its depth

$$\text{Im}\{\hat{p}(\eta_0)\} = \text{Im}\{\hat{p}_s\} \{1 + O(kz_0\delta^2)\}. \quad (5.28)$$

Similarly, across the shear stress layer, (5.17) shows that  $\text{Im}\{h\} = O(a\delta^2)$  and (A 9) shows that  $\text{Re}\{\hat{\tau}\} = O(aku_*^2)$  so that the pressure remains constant with only small variations:

$$\text{Im}\{\hat{p}(\eta_i)\} = \text{Im}\{\hat{p}_s\} \{1 + O(aku_*^2 kl_i)\} = \text{Im}\{\hat{p}_s\} \{1 + O(aku_*^2 \delta)\}. \quad (5.29)$$

Now, across the transition layer the pressure does vary significantly with height. First, the solution (5.11) shows that  $\text{Im}\{h\}$  has a contribution from  $h_t^{(3)}$ , which is of  $O(\delta)$ . However, this term contains  $\eta U_B'/U_B$  which is itself  $O(\delta)$  in the transition layer, and so overall the contribution to  $\text{Im}\{h\}$  is  $O(\delta^2)$ . The largest contribution to  $\text{Im}\{h\}$  is then from  $h_t^{(4)}$ , which is  $O(a\delta^{1+n})$ . The solution (A 6) shows that  $\text{Re}\{\hat{\tau}\} = O(aku_*^2)$ , which then gives a smaller contribution to  $\partial \hat{p}/\partial \eta$  than the contribution from  $\text{Im}\{h\}$ . Integration of the vertical momentum equation from the surface then shows that

$$\text{Im}\{\hat{p}(\eta_t)\} = \text{Im}\{\hat{p}_s\} - akU_1^2 2\kappa \delta^{1+2n} \{V_i - V e^{-\eta_t}(\eta_t + 1)\}. \quad (5.30)$$

Finally, in the upper layer the shear stress perturbation is exponentially small

because of the damping. The solution (5.7), together with the solutions for the coefficients from matching, shows that for fast waves  $\text{Im}\{h\} = \text{Im}\{\delta^2 H_2\} e^{-n}$  and for very fast waves  $\text{Im}\{h\} = \text{Im}\{\delta H_1\} e^{-n}$ , which can both be written  $\text{Im}\{h\} = \delta^2 H_i e^{-n}$ . Integration of the vertical momentum equation down from infinity then shows that

$$\text{Im}\{p(\eta_1)\} \sim -akU_B^2 \delta^2 H_i e^{-n}, \quad (5.31)$$

and the asymmetric part of the pressure decays with height according to potential flow. Tracing through the matching we find that for fast waves

$$H_i^{(f)} = \text{Im}\{H_2\} = \text{Im}\{T_9\} = \text{Im}\{I_5^{(f)}\}, \quad (5.32)$$

and for very fast waves

$$\delta H_i^{(vf)} = \text{Im}\{H_1\} = \text{Im}\{T_6\} = \text{Im}\{I_2^{(vf)}\}. \quad (5.33)$$

Both of these are the values of  $\text{Im}\{h\}$  at the top of the inner shear stress layer as  $\eta_i \rightarrow \infty$ . Hence the asymmetric pressure in the outer region develops because the streamlines at the top of the inner region are displaced asymmetrically about the wave. Finally, (5.23) and (5.26) show that

$$H_i^{(f)} = \frac{1}{2} \text{Im}\{I_3\} = -\frac{1}{V_i^2} \left( S_0 + \frac{2}{V_i^2} \right), \quad (5.34)$$

$$H_i^{(vf)} = -\frac{2\kappa}{\delta V_i} \left\{ \left( 1 + \frac{1}{V_i^2} \right) \text{Re} \left( \eta_i \frac{\partial K_0^*}{\partial \eta_i} \right)_s \right\}, \quad (5.35)$$

where  $S_0$  is the normalized surface stress given in (5.23).

The surface pressure is evaluated by matching (5.30) and (5.31) in their overlap, where  $k\eta = \delta^\alpha \eta_{ut}$  with  $\eta_{ut} = O(1)$  and  $0 < \alpha < n$ , in the limit  $\delta \rightarrow 0$ , which yields

$$\text{Im}\{\hat{p}_s\} = -ak \{ U_1 U_i 2\kappa \delta^{1+2n} + U_{ut}^2 \delta^2 H_i \}, \quad (5.36)$$

where  $U_{ut}$  is  $U_B$  evaluated in the overlap between the inner and outer region. Here we set this level to be at  $k\eta = \delta^\alpha$ , i.e. at  $\eta_{ut} = 1$ , and for definiteness we choose  $\alpha = \frac{1}{2}n$ . The precise value of  $k\eta$  is not important because  $U_B$  varies only logarithmically with height. Here we follow Hunt *et al.* (1988) and Belcher & Hunt (1993), who use the wind speed at the height of a middle layer,  $l_m$ , where  $kl_m = O((\delta/\kappa)^{1/2})$ . This length scale is then asymptotically between the length scales of the inner and outer regions. Hence we define  $U_m = U_B(l_m)$  and  $l_m = (\delta/\kappa)^{1/2}$ . Figure 2 shows the variation of  $kl_m$  with  $c/u_*$  when  $kz_0 = 10^{-4}$ .

Hence the asymmetric part of the surface pressure is written

$$\text{Im}\{\hat{p}_s\} = aku_*^2 \{ \beta + O(\delta^{2+n}) \} \quad (5.37)$$

where for fast waves  $\beta^{(f)} = \beta_{z_s}^{(f)} + \beta_{u_s}^{(f)} + \beta_0$  and

$$\beta_{z_s}^{(f)} = 2 \frac{U_m^2 U_1^2}{U_i^4} \left( 2 - \frac{c}{U_i} \right), \quad \beta_{u_s}^{(f)} = -2 \frac{U_m^2 c}{U_i^2 U_i}, \quad \beta_0 = 2\kappa \delta^{2n} \frac{U_i}{u_*}, \quad (5.38)$$

and for very fast waves  $\beta^{(vf)} = \beta_{z_s}^{(vf)} + \beta_{u_s}^{(vf)} + \beta_0$  where

$$\beta_{z_s}^{(vf)} = -2\kappa \frac{U_m^2 U_1^2}{u_* U_i^3} S_{K_0}, \quad \beta_{u_s}^{(vf)} = -2\kappa \frac{U_m^2}{u_* U_i} S_{K_0}, \quad (5.39)$$

where

$$S_{K_0} = \text{Re} \left\{ \frac{1}{K_{0s}^*} \left( \eta_i \frac{\partial K_0^*}{\partial \eta_i} \right)_s \right\}. \quad (5.40)$$

In the calculation of the wave growth rate it will be useful to have the solution for the surface stress (A 10), which is written here as

$$\operatorname{Re}\{\hat{\tau}_s\} = ak u_*^2 \{\gamma + O(\delta)\} \quad (5.41)$$

where for fast waves  $\gamma^{(f)} = \gamma_{z_s}^{(f)} + \gamma_{u_s}^{(f)}$  and

$$\gamma_{z_s}^{(f)} = 2 \frac{U_1^2}{U_i^2} \left(1 - \frac{c}{U_i}\right), \quad \gamma_{u_s}^{(f)} = -2 \frac{c}{U_i}, \quad (5.42)$$

and for very fast waves  $\gamma^{(vf)} = \gamma_{z_s}^{(vf)} + \gamma_{u_s}^{(vf)}$  and

$$\gamma_{z_s}^{(vf)} = -\frac{2\kappa U_1^2}{U_i u_*} S_{K_0}, \quad \gamma_{u_s}^{(vf)} = -\frac{2\kappa U_i}{u_*} S_{K_0}. \quad (5.43)$$

Numerical tests have shown that, for the parameters of interest here, the differences in the growth rates between fast and very fast waves are small, and so the results are plotted for fast waves only.

Comparison of these solutions for  $\beta$  and  $\gamma$  and the corresponding solutions for slow waves, which are listed in Appendix B, shows that the solutions are formally the same, except that the solutions for slow waves are missing the terms with factors of  $c/\bar{U}_i$ . For slow waves this factor is  $O(\delta)$ , and so these terms would be calculated at the next order, as was done explicitly by Belcher & Hunt (1993). Hence the main difference between the solutions for fast and slow waves is the different value of  $l_i$  that needs to be used in evaluating the formulae.

### 5.7. Discussion

The solutions derived here are valid provided the inner region is a thin layer, so that  $kl_i \ll 1$ . The conditions required to keep  $kl_i \ll 1$  were established in §4.2 and correspond to slow waves, with  $\kappa c/u_*$  of order one (when the solutions are quoted in Appendix B), and to fast waves, with  $\delta c/u_*$  of order one (when the solutions are quoted in Appendix A). The method cannot be used for wind waves in the intermediate regime because the inner region is no longer thin and also because the critical height is of the same order as the depth of the inner region, so that  $\bar{U}_i \approx c$  and the governing equation is singular. Resolution of this singularity requires explicit analysis of the critical layer, which is beyond the scope of this paper.

Some understanding of the solutions can be obtained by considering the streamline displacement,  $s(\xi, \eta)$ , at the 'top' of the inner region, at  $\eta = l_i$ , denoted here by  $s_i(\xi)$ . To estimate the magnitude of  $s_i(\xi)$  rearrange (2.2), which relates  $\tilde{u}$  and  $s$ , to give the streamline displacement in terms of the horizontal velocity perturbation

$$s_i(\xi) = z_s(\xi) - \int_{z_0}^{l_i} (\tilde{u}/U_B) d\eta. \quad (5.44)$$

The first term,  $z_s(\xi) = \operatorname{Re}\{a e^{ik\xi}\}$ , follows from the kinematic boundary condition that the wave surface is a streamline. Equation (5.44) expresses mass conservation across the inner region: if the air speeds up, so that  $\tilde{u} > 0$ , then the streamline is displaced downwards.

Now  $\tilde{u}$  can be estimated using the horizontal momentum equation (2.4). Since the inner region is thin,  $kl_i \ll 1$ , the pressure is approximately constant with height there, i.e.  $\tilde{p}(\xi, \eta) \approx \tilde{p}(\xi, z_0) \equiv \tilde{p}_s(\xi)$ . Hence combining (2.4) and (5.44) shows that  $s_i(\xi)$  can



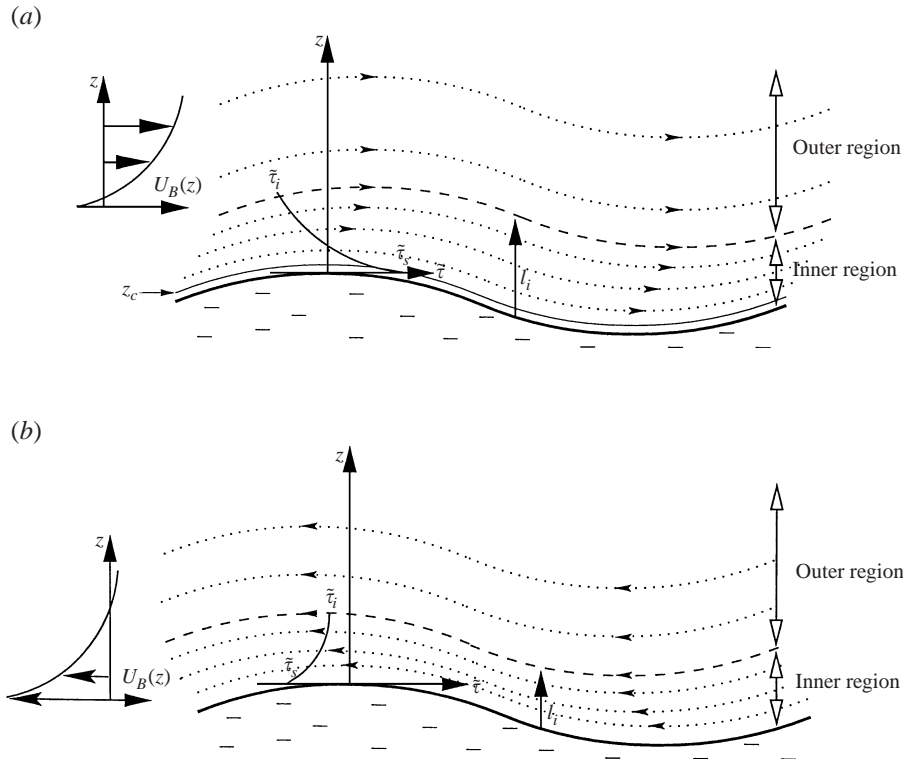


FIGURE 3. Sheltering over (a) slow and (b) fast waves.

be expressed as a sum of effects:

$$s_i(\xi) \approx z_s(\xi) + l_i \frac{\tilde{p}_s(\xi)}{U_i^2} + s_\tau(\xi), \tag{5.45}$$

namely displacement by the wave itself, a Bernoulli variation of streamline height associated with pressure variations (which tends to be negative at the wave crest, where the pressure is lowest and the air speeds are highest), and a displacement caused by the change in shear stress across the inner region, which is given by

$$s_\tau(\xi) = \int^{\xi} \frac{1}{U_B^2} \{ \tilde{\tau}_s(\xi) - \tilde{\tau}_i(\xi) \} d\xi. \tag{5.46}$$

Hence, deceleration of the air by a jump in wave-induced shear stress across the inner region,  $\tilde{\tau}_s - \tilde{\tau}_i$ , leads to reduced air speeds and hence upward streamline displacement.

The solutions  $\tilde{\tau} = O(aku_*^2)$ , show that  $s_\tau \sim (u_*^2/U_i^2)/k \sim (u_*/U_i)l_i$ , which is a factor  $u_*/U_1$  smaller than the other two terms and so the streamline displacement at the top of the inner region,  $s_i$ , is largely independent of the turbulent stress. In the outer region the wave-induced stress is negligible and so again the streamline displacement, which towards the surface matches the value at the top of the inner region, is largely independent of the turbulent stress and to a good approximation is just an exponential decay.

Although small,  $s_\tau$  is important. It is related, via (5.46), to the integral along a streamline of the jump in wave-induced stress across the inner region. Hence, as an air parcel moves along a streamline the frictional deceleration from the jump in wave-induced turbulent stress leads to an accumulated displacement of the streamline that

leads to the smallest wind speeds, and hence the maximum streamline displacement, being downwind of the wave crest. Belcher & Hunt (1993) called this process *non-separated sheltering*. For slow waves, the basic flow in the inner region is from left to right, i.e. in the same direction as the wave propagates, and so the displacement in the streamlines is to the right of the wave crest (figure 3a), but for fast waves the basic flow in the inner region is from right to left, i.e. against the direction of propagation, and the streamlines are displaced slightly to the left (figure 3b). This small displacement of streamlines at the top of the inner region also means that streamlines in the outer region are displaced slightly downwind of the wave crest. The pressure perturbation that develops in the outer region then has its minimum displaced downwind of the wave crest, which leads to the contribution to the surface pressure denoted by  $\beta_z$ . Orbital motions at the wave surface also lead to a jump in wave-induced stress across the inner region that is negative and leads to a sheltering displacement of the streamline at the top of the inner region upwind of the wave crest. This process leads to a small shift in the surface pressure denoted by  $\beta_{\tilde{u}_s}$ . Finally, in the lower part of the outer region a small wave-induced pressure gradient develops to balance the small wave-induced stress gradient. This leads to an additional shift in the surface pressure minimum away from the wave crest, namely  $\beta_0$ .

There are interesting differences between the sheltering for fast and slow waves. When the waves are slow the surface stress is positive,  $\tilde{\tau}_s > 0$ , and the stress at the top of the inner region is negative,  $\tilde{\tau}_i < 0$ . Hence the jump in stress,  $\tilde{\tau}_s - \tilde{\tau}_i$ , is large, so there is a strong sheltering effect and substantial values of  $\beta_z$ . In contrast, when the waves are fast the wind near the surface is against the direction of wave propagation so the wave-induced surface stress is negative,  $\tilde{\tau}_s < 0$ . The stress at the top of the inner region remains negative,  $\tilde{\tau}_i < 0$ . The net jump in stress across the inner region is therefore much smaller and the sheltering is weaker.

## 6. Growth and decay of the waves

The wave-induced pressure and stress do work at the wave surface, which then leads to an energy flux into or out of the wave motions, thence leading to wave growth or decay. Following Davis (1972) and Belcher & Hunt (1993), an equation can be formed for the wavelength-averaged energy in the wave motions,  $\tilde{E}$ . If only the leading-order quadratic terms are retained then three sources of work change  $\tilde{E}$ , namely

$$\frac{\partial \tilde{E}}{\partial t} = \langle \tilde{\sigma}_{ij} \tilde{u}_i n_j \rangle = \langle -c \{ -\tilde{p}_s + \tilde{\tau}_{33s} \} dz_s / d\zeta \rangle + \langle \tilde{\tau}_s \tilde{u}_s \rangle, \quad (6.1)$$

where  $\langle \rangle$  denotes average over a wavelength,  $\tilde{\sigma}_{ij}$  is the wave-induced stress tensor, and  $n_j = (-dz_s/d\zeta, 1)$  is the normal to the surface (to the leading-order approximation). The kinematic boundary condition  $\tilde{w}_s = Dz_s/Dt = -c dz_s/dx$  was used in evaluating the first term on the right of (6.1). The contribution from the normal stress term is small,  $-c \langle \tilde{\tau}_{33s} dz_s/d\zeta \rangle$ , (cf. Belcher & Hunt 1993; Mastenbroek 1996) because it requires surface stress perturbations in phase with wave slope, which are smaller than perturbations in phase with the elevation (Cohen 1997), and so is neglected here. Hence two terms need to be evaluated.

The first term,  $c \langle \tilde{p}_s dz_s/d\zeta \rangle$ , can be evaluated using the solution for the asymmetric surface pressure (5.37) to yield

$$c \langle \tilde{p}_s dz_s/d\zeta \rangle = \frac{1}{2} (ak)^2 u_*^2 c \beta, \quad (6.2)$$

where  $\beta$  is given by (5.38). The second term in (6.1),  $\langle \tilde{\tau}_s \tilde{u}_s \rangle$ , can be evaluated once the horizontal motions at the surface are specified. For deep-water gravity waves with the solution for the surface stress (5.41) this term gives

$$\langle \tilde{\tau}_s \tilde{u}_s \rangle = \frac{1}{2}(ak)^2 u_*^2 c \gamma, \quad (6.3)$$

where  $\gamma$  is given in (5.42).

The wavelength-averaged energy in a deep-water wave is  $\tilde{E} = \frac{1}{2}(\rho_w/\rho_a)ga^2$ , with the current normalization that the density of air is one (Phillips 1977, p. 39), so that

$$\frac{\partial \tilde{E}/\partial t}{\tilde{E}} = \frac{\rho_a}{\rho_w} \left( \frac{u_*}{c} \right)^2 \sigma(\beta + \gamma), \quad (6.4)$$

where  $\sigma = ck$  is the radian wave frequency. Hence the waves grow or decay exponentially in time, with an e-folding time given by the reciprocal of the right-hand side of (6.4).

The expression obtained here for the e-folding time of the waves has a similar form to that found by previous investigators from Miles (1957) onwards and found in data (Plant 1984). It is proportional to the ratio of the water to air densities, increases quadratically with wind speed, through the  $u_*^2$  term, because it scales on the surface stress in the basic state wind profile which controls the strength of the sheltering. For a deep-water wave, (6.4) decreases with increasing wavelength, since  $\sigma/c^2 = (k^3/g)^{1/2}$ . The factor, denoted here  $(\beta + \gamma)$ , has been intensely debated in the literature. It is this factor that we now discuss and compare with previous studies and data.

In this linear analysis the value of the growth-rate coefficient,  $(\beta + \gamma)$ , does not vary with wave slope, but it does vary with the relative wind speed,  $c/u_*$ , with the relative surface roughness  $kz_0$  and with the rate of damping of the mixing-length model,  $n$ , see (3.5). First consider the variation with the damping rate,  $n$ . Strictly  $0 < n < 1$ , but consider the limit  $n \rightarrow 0$ , which is the limit of no damping, so that the mixing-length model is allowed to operate right up through the outer region. Although according to the scaling arguments given in §3 such a mixing-length model is inappropriate in the outer region, this limit does allow comparison with previous studies. Hence in the limit  $n \rightarrow 0$  the pressure asymmetry associated with the outer-region stress is

$$\beta_0 \rightarrow 2\kappa(\bar{U}_i - c)/u_*. \quad (6.5)$$

This is the value of the growth-rate coefficient obtained by Jacobs (1987), who used an eddy-viscosity model for the wave-induced shear stress throughout the flow and considered only slow waves. The analysis here shows how, even when a mixing-length model is used throughout the flow, there are additional contributions to  $\beta$  from inner-region effects (i.e.  $\beta_{z_s}$  and  $\beta_{\tilde{u}_s}$ ) and also from the surface-stress effects (i.e.  $\gamma_{z_s}$  and  $\gamma_{\tilde{u}_s}$ ). We have also shown that this result also applies to fast waves.

In the limit of strong damping, when the shear stress is damped rapidly to zero in the outer region, namely when  $n \rightarrow 1$ , and for slow waves, the solutions obtained here tend to the solutions found by Belcher & Hunt (1993), who simply set the mixing-length model to zero above the inner region. Hence the discontinuity in the solutions of Belcher & Hunt (1993) for the stress perturbation at the top of the inner region is not important for practical purposes when calculating the wave growth rate.

As  $n$  increases from very small values,  $\beta_0$  reduces. When  $n > \frac{1}{2}$  the  $\beta_0$  contribution has a smaller magnitude than  $\beta_{z_s}$  and  $\beta_{\tilde{u}_s}$ . Figure 4 shows the variation of  $\beta$  with  $c/u_*$  for  $n = 0, \frac{1}{2}$  and 1. The theoretical curves for slow waves are truncated when the depth of the inner region reaches its value at the bifurcation, namely  $kl_i = 2\kappa^2$ , which yields a maximum of  $c/u_* = \{\ln(2\kappa^2/kz_0) - 1\}/\kappa$  (see figure 2). The theoretical curve

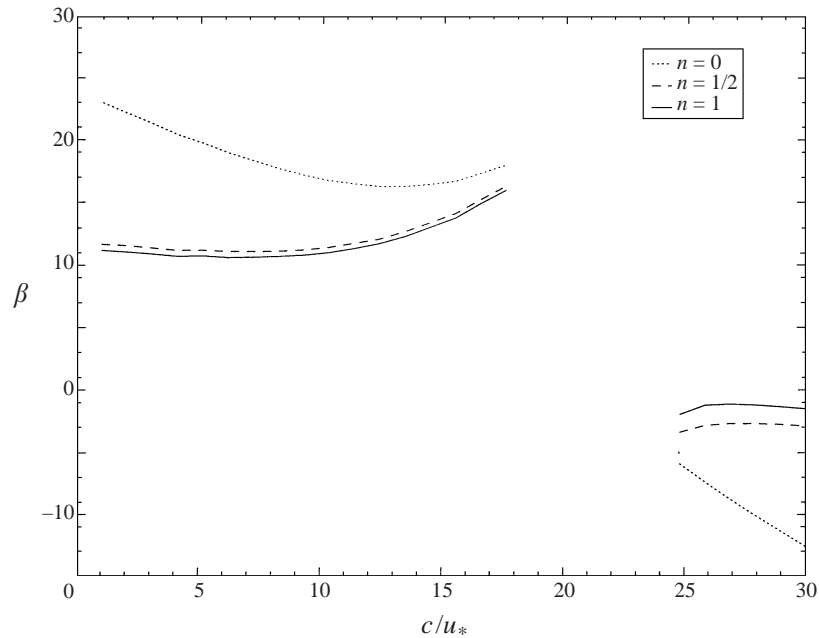


FIGURE 4. Variation of  $\beta$  with wind-wave speed for different damping of the mixing-length model ( $kz_0 = 10^{-4}$ ).

for fast waves is begun when  $\delta/\kappa = 1$  (see figure 2). It is clear from these plots that, although  $\beta_0$  is formally of the same magnitude as  $\beta_{z_s}$  and  $\beta_{\bar{u}_s}$  when  $0 < n < \frac{1}{2}$ , the numerical value of  $\beta_0$  is smaller than the two other terms when  $n = \frac{1}{2}$ . We conclude that for values of  $n$  that correctly damp the mixing-length model in the outer region, i.e.  $0 < n < \frac{1}{2}$ ,  $\beta$  is dominated by  $\beta_{z_s}$  and  $\beta_{\bar{u}_s}$  that are associated with sheltering in the inner region. This conclusion agrees with the findings of Harris *et al.* (1996), who computed  $\beta$  using a damped  $k - \varepsilon$  model for stationary waves and found that the results are insensitive to the damping rate beyond a threshold.

Van Duin (1996) developed an analytical model for growth of slow waves based on similar assumptions to the model developed here, but with an eddy viscosity that is algebraically damped in the outer region (rather than exponentially damped as here). In the limit that  $kz_0 \rightarrow 0$  and  $\kappa c/u_* \rightarrow 0$ , when  $U_m$  and  $U_i \rightarrow U_1$ , the present results yield

$$\beta \rightarrow 4(1 - c/\bar{U}_1) + \beta_0. \quad (6.6)$$

The first term, which comes from  $\beta_{z_s} + \beta_{\bar{u}_s}$ , is the same as the second term in van Duin's equation (4.3). The final term obtained here, namely  $\beta_0$ , corresponds to the last term in van Duin's (4.3), but differs in detail because we have used different forms for the damping (algebraic in van Duin, see his equation (2.4); exponential here, see equation (3.5)). Van Duin's (4.3) has an additional term of  $-2$ . We have been unable to establish the origin of this term in van Duin's calculations. He evaluated his formula to obtain a value of  $\beta$  in the range 3–4: much smaller than the values obtained here. The reason for the smaller values is that van Duin's method does not account for the shear in the approach flow, which yields the factors of  $U_m/U_i$  in our approach (5.38). These factors, when raised to the powers of 2 or 4 as they are in our (5.38), are numerically large and account for our larger values.

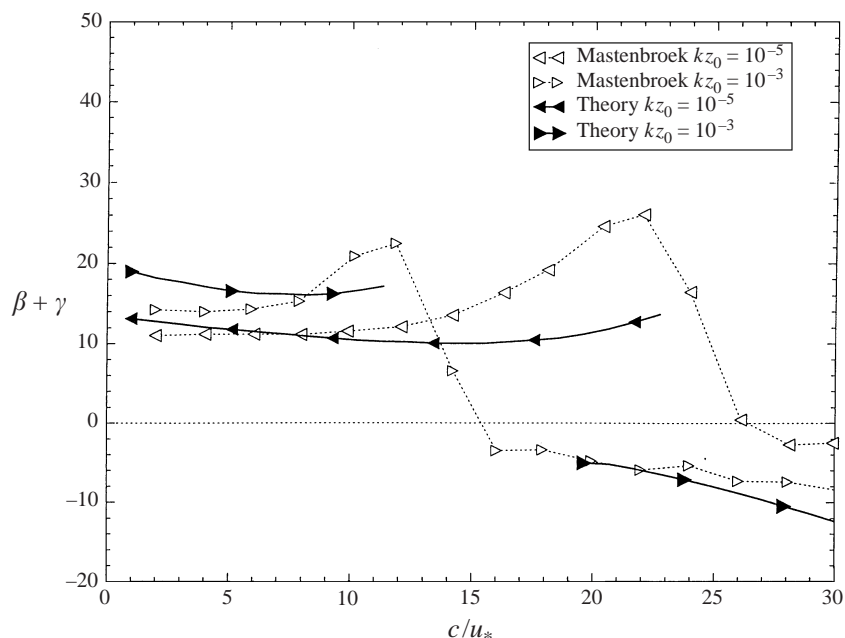


FIGURE 5. Comparison of the present theory with computations by Mastenbroek (1996).

Evidence that these factors of  $U_m/U_i$  are accurate comes from figure 5, which shows comparisons between values of the growth-rate coefficient,  $\beta + \gamma$ , calculated using the present theory with full damping,  $n = 1$ , and values computed numerically by Mastenbroek (1996), who used a full second-order closure model to parameterize the turbulent stress. The criterion for fast waves, namely  $\delta/\kappa > 1$ , yields  $c/u_* > 31$  when  $kz_0 = 10^{-5}$  and so no theoretical curve is shown for fast waves in this case.

Figure 5 shows that the present solutions agree well with Mastenbroek's fully nonlinear computations for both fast and slow waves. The theory shows both the same variation with  $c/u_*$  and also the same variation with the relative roughness  $kz_0$ , which suggest that the factors containing  $U_m/U_i$  are accurate. Agreement between the computations and the theory is particularly satisfying because we have argued in §3 that the damped mixing-length model used here captures the essence of the physics parameterized in a full second-order closure. The results in figure 5 support this claim. Separate evaluation of the contributions to the growth-rate coefficient (Cohen 1997) shows that it is the contribution from  $\beta_{z_s}$ , i.e. the contribution from sheltering, that dominates for slow waves (in agreement with Belcher & Hunt 1993). In the slow-wave regime the results computed by Mastenbroek are larger than the theoretical values as  $c/u_*$  approaches its maximum value for slow waves. At these larger values of  $c/u_*$  the small parameter  $\delta/\kappa$  becomes larger and the asymptotic solutions are not so accurate. Physically, the critical-layer mechanism might be contributing to wave growth at these more intermediate wave speeds. Nevertheless, the value of  $c/u_*$  that corresponds to the maximum value of  $\beta + \gamma$  computed by Mastenbroek corresponds well with the maximum value of  $c/u_*$  in the slow-wave regime, which should be a useful practical result. The present work also shows that it is the contribution from  $\gamma_{z_s}$ , i.e. the work of the wave-induced shear stress at the surface, that dominates for fast waves (the sheltering term is small for fast waves as explained in §5.7). The fast-wave theory agrees well with the computations when  $kz_0 = 10^{-3}$  and  $20 < c/u_* < 25$ . For larger

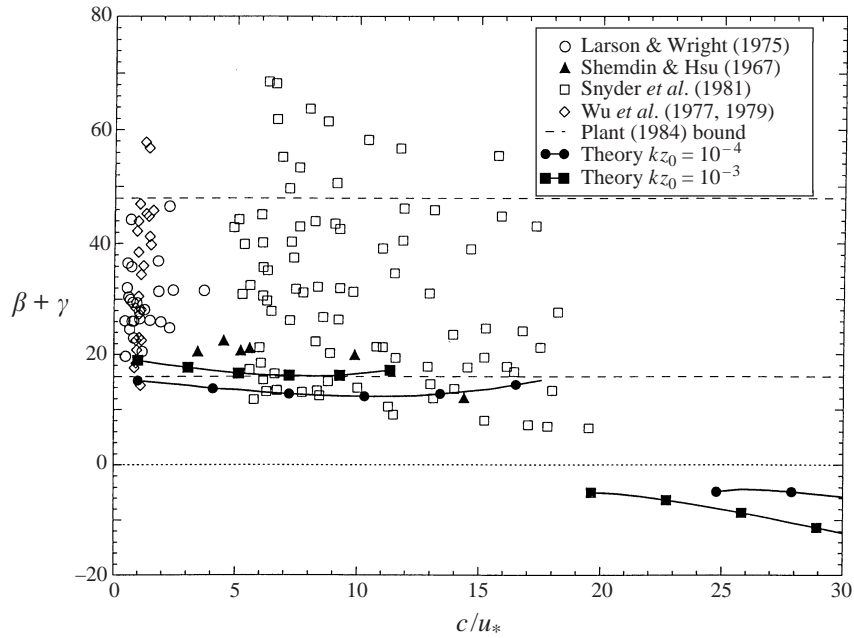


FIGURE 6. Comparison of the present theory with data collated by Plant (1984).

values the agreement is not as good, probably because parameters are moving into the very fast regime.

The values of the growth-rate coefficient for the fast waves are smaller than for the slow waves. The actual e-folding times for decay of fast waves are even longer. Recall from (6.4) that the energy contained in the wave motions increases or decreases exponentially in time and the e-folding time is

$$t_e = \frac{\rho_w}{\rho_a} \frac{1}{\sigma} \left( \frac{c}{u_*} \right)^2 \frac{1}{|\beta + \gamma|}. \quad (6.7)$$

For given values of the wind speed  $U_1 = (u_*/\kappa) \ln 1/kz_0$ , wind-wave parameter,  $c/u_*$ , and relative roughness,  $kz_0$ , the wave phase speed can be determined and hence, on using the linear dispersion relation  $c^2 = g/k$ , so can the wavenumber  $k$  and wavelength  $2\pi/k$ , of the waves. For example, if  $U_1 = 10 \text{ m s}^{-1}$  and  $kz_0 = 10^{-4}$ , then  $u_* \approx 0.43 \text{ m s}^{-1}$ . A slow-wave case with  $c/u_* = 5$ , then yields  $c \approx 2 \text{ m s}^{-1}$  and  $\lambda \approx 4 \text{ m}$  and so for the air–sea interface, with  $\rho_w/\rho_a \approx 800$  the e-folding time for wave growth is  $t_e \approx 300 \text{ s}$ , i.e. 5 minutes. In contrast, a fast-wave case with  $c/u_* = 30$ , then yields  $c \approx 15 \text{ m s}^{-1}$  and  $\lambda \approx 140 \text{ m}$  and so  $t_e \approx 11.4 \times 10^5 \text{ s}$ , i.e. about 30 hours. We are not dismayed by this value: it has long been known that long-wavelength swell can propagate long distances without significant dissipation (Ursell 1954). The long time scales arise from the large values of  $c/u_*$ , whose square multiplies the e-folding time.

Finally, figure 6 shows comparisons of values of the growth-rate coefficient from the theory with values from laboratory and open-ocean experiments collated by Plant (1984). (Belcher, Harris & Street 1994, show these data as originally plotted by Plant and then also plotted as in figure 6.) The data lie in the slow- and intermediate-wave regimes. As has been reported by others (e.g. Mastenbroek *et al.* 1996; Belcher & Hunt 1998) the theoretical values are smaller than the measurements. We can offer

no new explanation of this, except to point out that the values measured by Shemdin & Hsu (1967) do lie close to the theory. This is significant because Shemdin & Hsu measured growth of wind-ruffled paddle-generated waves – a configuration that is close to the configuration modelled in the present theory. In contrast the remaining measurements in figure 6 implied the growth rate of purely wind-generated waves, which are strongly influenced by nonlinear wave–wave interactions and wave breaking (e.g. Phillips 1977, § 4.6).

Hasselmann & Bosenberg (1991) made measurements on the ocean over a wide range of  $c/u_*$  to determine the growth or decay rates of the waves. They state that from their observations they could not detect either growth or decay of fast waves. What they found was that when the waves travel faster than  $U_B(k^{-1})$  the absolute value of what we call  $|(u_*/c)^2(\beta + \gamma)|$  is less than 0.03. The theory presented here shows that when  $kz_0 = 10^{-3}$  this factor is about 0.0125 when  $c/u_* = 20$ , so that with only three times the accuracy of their experiment, decay of fast waves should be measurable. Perhaps the time has come to conduct new experiments.

## 7. Conclusions

Air flow over waves is usefully divided into two regions. Close to the interface is an inner region where the wave-induced turbulent shear stress significantly affects the wave-induced mean flow, which leads to a sheltering effect, whereby streamlines are displaced asymmetrically about the wave crest. In an outer region, turbulence is advected over a wavelength too rapidly for it to transport significant momentum and so the wave-induced flow there is inviscid to a good approximation. There are three parameter regimes that are distinguished by the relative wind and wave speeds,  $c/u_*$ . In the slow-wave regime, where  $\kappa c/u_*$  is of order one, the critical height,  $z_c$ , where the mean wind speed equals the wave phase speed, lies very close to the surface, within the inner surface layer and plays no significant dynamical role in the flow. In the fast-wave regime, where  $\delta c/u_*$  is of order one, the critical height lies well above the inner region, and too far from the surface to have a significant dynamical effect. In the intermediate regime, where  $20 < c/u_* < 25$  (if  $kz_0 = 10^{-4}$ ), the critical layer is towards the top of the inner region and probably plays a significant dynamical role, although further work is needed to clarify the combined effects of sheltering and the critical layer in this regime.

Here we have analysed air flow over slow and fast waves by calculating the displacement of streamlines as they pass over the wave. The streamline displacement at the top of the inner region is controlled by three processes: displacement over the wave surface, a Bernoulli displacement associated with pressure variations, and a small, but important, asymmetric displacement due to the turbulent shear stress. This asymmetric displacement of streamlines leads to sheltering downwind of the wave crest. Above the inner region, in the outer region, the streamline displacement remains in phase with the streamline at the top of the inner region: no further asymmetry is produced because the wave-induced shear-stress gradient there is too weak. A pressure perturbation then develops in the outer region that has its minimum displaced downwind of the wave crest. This pressure perturbation together with the surface stress perturbation does work at the wave surface and leads to growth of slow waves and decay of fast waves.

There is hope that the present formulation, wherein the streamline displacement is analysed, can shed light onto the intermediate-wave regime, where there is a dynamical effect of the critical layer in addition to the sheltering caused by the turbulent shear

stress, because Belcher *et al.* (1998) have shown how an inviscid critical layer can be analysed in this framework.

Values of the wave growth rate calculated from the analysis agree well with computations of Mastenbroek (1996) and with the laboratory data for slow and intermediate waves of Shemdin & Hsu (1967), but other experiments report values that are larger than the theoretical values by a factor of about two. It is time to re-evaluate these data and perhaps also time to perform further experiments, particularly to produce data for decay of fast waves.

The e-folding time for decay of fast waves is very long: a day or more for the values chosen in §6. So why should this wind-induced decay be significant? As we suggested in the introduction, one application of this theory for interaction between wind and fast waves is in the dynamics of the spectrum of fully-developed sea. When the sea state is fully developed, nonlinear interactions transfer wave energy away from the peak in the spectrum into both higher- and lower-frequency waves (Komen, Hasselmann & Hasselmann 1984). Now, the peak in the spectrum corresponds to waves that travel at the wind speed, so that lower-frequency waves are travelling faster than the wind. So, according to the present calculations, these low-frequency waves lose energy to the wind. The slopes of these low-frequency waves are so small that breaking must be at most very rare. Hence, if there is an equilibrium, this loss of energy to the wind might balance the energy gained at these low frequencies by nonlinear interactions.

It is a pleasure to thank Julian Hunt and Nigel Wood for useful discussions and suggestions during the course of this work. J.E.C. is grateful to NERC for funding under a CASE studentship with the UK Met. Office. Funding for the completion of this work was provided by the EC under the ASPEN project, contract ENV4-CT97-0460.

## Appendix A. Solutions for fast waves

### A.1. Upper layer

In the upper layer  $\eta = \eta_1/k$ , where  $\eta_1 = O(1)$ , and solutions are

$$\hat{u} \sim akU_B e^{-\eta_1} + O(\delta), \quad (\text{A } 1)$$

$$\hat{w} \sim ak iU_B e^{-\eta_1} + O(\delta), \quad (\text{A } 2)$$

$$\hat{\tau} \sim O(ak e^{-1/\delta}). \quad (\text{A } 3)$$

### A.2. Transition layer

In the transition layer  $\eta = \eta_t \delta^n/k$ , where  $\eta_t = O(1)$ , and solution are

$$\hat{u} \sim ak \frac{U_1^2}{U_B} \left\{ 1 - \delta^n \int^{\eta_t} V^2(y) dy + O(\delta) \right\}, \quad (\text{A } 4)$$

$$\hat{w} \sim ak iU_B \left\{ 1 - \delta^n \int^{\eta_t} \frac{dy}{V^2(y)} + O(\delta^{2n}, \delta^{n+1}) \right\}, \quad (\text{A } 5)$$

$$\hat{\tau} \sim -2ak u_*^2 \frac{e^{-\eta_t}}{V^2} \{1 + O(\delta)\}. \quad (\text{A } 6)$$



A.3. Inner shear stress layer

In the inner shear stress layer  $\eta = \eta_i l_i$ , where  $\eta_i = O(1)$ , and solutions are

$$\hat{u} \sim akU_1 \left[ \frac{1}{V_i} + \frac{\delta}{\kappa} \left\{ \left( S_0 + \frac{2}{V_i^2} \right) K_0^*(X) + \frac{1}{V_i^2} \ln \eta_i - 2\kappa^2(\eta_i + i) \right\} + O(\delta^2) \right], \quad (A 7)$$

$$\hat{w} \sim ak i U_1 \left[ V_i - \delta \left\{ \frac{2\kappa}{V_i^2} \eta_i + \frac{1}{\kappa} \ln \eta_i \right\} + O(\delta^2) \right], \quad (A 8)$$

$$\hat{\tau} \sim -2aku_*^2 \left[ \left( S_0 + \frac{2}{V_i^2} \right) \eta_i \frac{\partial K_0^*}{\partial \eta_i} + \frac{1}{V_i^2} - 2\kappa^2 \eta_i + O(\delta) \right], \quad (A 9)$$

where

$$\frac{1}{2} S_0 = \frac{(\bar{U}_1 - c)^2}{\bar{U}_i(\bar{U}_i - c)} - \frac{c}{\bar{U}_i}. \quad (A 10)$$

A.4. Inner surface layer

In the inner surface layer  $\eta = \eta_0 z_0$ , where  $\eta_0 = O(1)$ , and solutions are

$$\hat{u} \sim ak \left\{ c + \frac{1}{2} S_0 \frac{u_*}{\kappa} \ln \eta_0 + O(u_* k z_0) \right\}, \quad (A 11)$$

$$\hat{w} \sim ak ic \{ 1 + O(k z_0) \}, \quad (A 12)$$

$$\hat{\tau} \sim aku_*^2 \{ S_0 + O(k z_0 / \delta^2) \}. \quad (A 13)$$

A.5. Inner region for very fast waves

To the order listed, solutions in the outer region are the same for very fast waves as for fast waves. Hence, only solutions in the inner region need to be listed here:

$$\hat{u} \sim akU_B \left[ \frac{1}{V_i^2} + \left( 1 + \frac{1}{V_i^2} \right) \frac{K_0^*(X)}{K_{0s}^*} + O(\delta) \right], \quad (A 14)$$

$$\hat{w} \sim ak i U_B \left[ 1 + \delta \left\{ I_1 \eta_i + I_2 + I_3 \eta_i \frac{\partial K_0^*}{\partial \eta_i} \right\} + O(\delta^2) \right], \quad (A 15)$$

$$\hat{\tau} \sim ak 2\kappa u_* U_B \frac{1}{K_{0s}^*} \left( 1 + \frac{1}{V_i^2} \right) \eta_i \frac{\partial K_0^*}{\partial \eta_i}, \quad (A 16)$$

where  $I_1, I_2$  and  $I_3$  are given in (5.25) and (5.26). The surface stress is

$$\hat{\tau} \rightarrow -2ak\kappa u_* c \frac{1}{K_{0s}^*} \left( 1 + \frac{1}{V_i^2} \right) \left( \eta_i \frac{\partial K_0^*}{\partial \eta_i} \right)_s. \quad (A 17)$$

**Appendix B. Solutions for slow waves**

Solutions in the outer region are formally the same for slow and fast waves. Any differences are accounted for automatically by the different sign of  $U_B$ , which is positive for fast waves and negative for slow waves. Hence we list here only the solutions in the inner region, which do differ.

B.1. Inner shear stress layer

In the inner shear stress layer  $\eta = \eta_i l_i$ , where  $\eta_i = O(1)$ , and solutions are

$$\hat{u} \sim akU_1 \left[ \frac{1}{V_i} - \frac{\delta}{\kappa} \left\{ \left( S_0 + \frac{2}{V_i^2} \right) K_0(X) + \frac{1}{V_i^2} \ln \eta_i + 2\kappa^2(\eta_i - i) \right\} + O(\delta^2) \right], \quad (B 1)$$

$$\hat{w} \sim ak i U_1 \left[ V_i - \delta \left\{ \frac{2\kappa}{V_i^2} \eta_i - \frac{1}{\kappa} \ln \eta_i \right\} + O(\delta^2) \right], \quad (\text{B } 2)$$

$$\hat{\tau} \sim -2aku_*^2 \left[ \left( S_0 + \frac{2}{V_i^2} \right) \eta_i \frac{\partial K_0}{\partial \eta_i} + \frac{1}{V_i^2} + 2\kappa^2 \eta_i + O(\delta) \right], \quad (\text{B } 3)$$

where

$$S_0 = \frac{2}{V_i^2}. \quad (\text{B } 4)$$

### B.2. Inner surface layer

In the inner surface layer  $\eta = \eta_0 z_0$ , where  $\eta_0 = O(1)$ , and solutions are

$$\hat{u} \sim ak \left\{ c + \frac{1}{2} S_0 \frac{u_*}{\kappa} \ln \eta_0 + O(u_* k z_0) \right\}, \quad (\text{B } 5)$$

$$\hat{w} \sim ak ic \{ 1 + O(k z_0) \}, \quad (\text{B } 6)$$

$$\hat{\tau} \sim aku_*^2 \{ S_0 + O(k z_0 / \delta^2) \}. \quad (\text{B } 7)$$

### B.3. Asymmetric pressure and shear stress at the surface

Calculation of the pressure variation through the flow as in §5.6 shows that for slow waves

$$\text{Im}\{\hat{p}_s\} = aku_*^2 \{ \beta + O(\delta^{2+n}) \} \quad (\text{B } 8)$$

where  $\beta = \beta_{z_s} + \beta_{u_s} + \beta_o$  and

$$\beta_{z_s} = 4 \frac{U_m^2 U_1^2}{U_i^4}, \quad \beta_{u_s} = O(\delta), \quad \beta_o = 2\kappa \delta^{2n} \frac{U_i}{u_*}. \quad (\text{B } 9)$$

The surface stress is given by

$$\text{Re}\{\hat{\tau}_s\} = aku_*^2 \{ \gamma + O(\delta) \} \quad (\text{B } 10)$$

where  $\gamma = \gamma_{z_s} + \gamma_{u_s}$  and

$$\gamma_{z_s} = 2 \frac{U_1^2}{U_i^2}, \quad \gamma_{u_s} = O(\delta). \quad (\text{B } 11)$$

## REFERENCES

- ABRAMOWITZ, M. & STEGUN, I. R. 1972 *A Handbook of Mathematical Functions*. Dover.
- BELCHER, S. E., HARRIS, J. A. & STREET, R. L. 1994 Linear dynamics of wind waves in coupled turbulent air–water flow. Part 1. Theory *J. Fluid Mech.* **271**, 119–151.
- BELCHER, S. E. & HUNT, J. C. R. 1993 Turbulent shear flow over slowly moving waves. *J. Fluid Mech.* **251**, 109–148.
- BELCHER, S. E. & HUNT, J. C. R. 1998 Turbulent flow over hills and waves. *Ann. Rev. Fluid Mech.* **30**, 507–538.
- BELCHER, S. E., HUNT, J. C. R. & COHEN, J. E. 1998 Turbulent shear flow over growing waves *Proc. IMA Conference on Wind–Wave Interactions* (ed. S. Sajjadi, N. H. Thomas & J. C. R. Hunt). Oxford (to appear).
- BELCHER, S. E., NEWLEY, T. M. J. & HUNT, J. C. R. 1993 The drag on an undulating surface induced by the flow of a turbulent boundary layer. *J. Fluid Mech.* **249**, 557–596.
- BRITTER, R. E., HUNT, J. C. R. & RICHARDS, K. J. 1981 Air flow over a 2-d hill: studies of velocity speed up, roughness effects and turbulence. *Q. J. R. Met. Soc.* **107**, 91–110.
- COHEN, J. E. 1997 Theory of turbulent wind over fast and slow waves. PhD thesis, University of Cambridge.

- DAVIS, R. E. 1972 On prediction of turbulent flow over a wavy boundary. *J. Fluid Mech.* **52**, 287–306.
- DUIN, C. A. VAN 1996 Rapid-distortion turbulence models in the theory of surface-wave generation. *J. Fluid Mech.* **329**, 147–153.
- DUIN, C. A. VAN & JANSSEN, P. A. E. M. 1992 An analytic model of the generation of surface gravity waves by turbulent air flow. *J. Fluid Mech.* **236**, 197–215.
- HARRIS, J. A., BELCHER, S. E. & STREET, R. L. 1996 Linear dynamics of wind-waves in coupled turbulent air-water flow. Part 2. Numerical model. *J. Fluid Mech.* **308**, 219–254.
- HASSELMANN, D. & BOSENBERG, J. 1991 Field measurements of wave-induced pressure over wind-sea and swell. *J. Fluid Mech.* **230**, 391–428.
- HUNT, J. C. R., LEIBOVICH, S. & RICHARDS, K. J. 1988 Turbulent shear flow over low hills. *Q. J. R. Met. Soc.* **114**, 1435–1471.
- HUNT, J. C. R. & RICHARDS, K. J. 1984 Stratified airflow over one or two hills. *Boundary-Layer Met.* **30**, 223–259.
- JACOBS, S. J. 1987 An asymptotic theory for the turbulent flow over a progressive wave. *J. Fluid Mech.* **174**, 69–80.
- JACKSON, P. S. & HUNT, J. C. R. 1975 Turbulent wind flow over a low hill. *Q. J. R. Met. Soc.* **101**, 929–955.
- JEFFREYS, H. 1925 On the formation of water waves by wind. *Proc. R. Soc. Lond. A* **107**, 189–206.
- KOMEN, G. J., CAVALERI, L., DONELAN, M., HASSELMANN, K., HASSELMAN, S. & JANSSEN, P. A. E. M. 1994 *Dynamics and Modelling of Ocean Waves*. Cambridge University Press.
- KOMEN, G. J., HASSELMANN, K. & HASSELMANN, S. 1984 On the existence of a fully developed windsea spectrum. *J. Phys. Oceanogr.* **14**, 1271–1285.
- LIGHTHILL, M. J. 1957 The fundamental solution for small steady three-dimensional disturbances to a two-dimensional parallel shear flow. *J. Fluid Mech.* **3**, 113–144.
- LOMBARDI, P., DE ANGELIS, V. & BANNERJEE, S. 1996 Direct numerical simulation of near-interface turbulence in coupled gas-liquid flow. *Phys. Fluids* **8**, 1643–1665.
- MAKIN, V. K., KUDRYAVSTEV, V. N. & MASTENBROEK, C. 1995 Drag of the sea surface. *Boundary-Layer Met.* **73**, 159–182.
- MASTENBROEK, C. 1996 Wind-wave interaction. PhD thesis, Delft Technical University.
- MASTENBROEK, C., MAKIN, V. K., GARAT, M. H. & GIOVANANGELI, J. P. 1996 Experimental evidence of the rapid distortion of the turbulence in the air flow over water waves. *J. Fluid Mech.* **318**, 273–302.
- MILES, J. W. 1957 On the generation of surface waves by shear flows. *J. Fluid Mech.* **3**, 185–204.
- MILES, J. W. 1993 Surface-wave generation revisited. *J. Fluid Mech.* **256**, 427–441.
- MILES, J. W. 1996 Surface-wave generation: a viscoelastic model. *J. Fluid Mech.* **322**, 131–145.
- PHILLIPS, O. M. 1977 *The Dynamics of the Upper Ocean*. Cambridge University Press.
- PIERSON, W. J. & MOSKOWITZ, L. 1964 A proposed spectral form for fully developed wind seas based on the similarity theory of S. A. Kitaigorodskii. *J. Geophys. Res.* **69**, 5181–5190.
- PLANT, W. J. 1984 A relationship between wind shear stress and wave slope. *J. Geophys. Res.* **87**, C3, 1961–1967.
- SHEMDIN, O. H. & HSU, E. Y. 1967 The dynamics of wind in the vicinity of progressive water waves. *J. Fluid Mech.* **30**, 403–416.
- SYKES, R. I. 1980 An asymptotic theory of incompressible turbulent flow over a small hump. *J. Fluid Mech.* **101**, 647–670.
- TOWNSEND, A. A. 1961 Equilibrium layers and wall turbulence. *J. Fluid Mech.* **11**, 97–120.
- TOWNSEND, A. A. 1972 Flow in a deep turbulent boundary layer disturbed by water waves. *J. Fluid Mech.* **55**, 719–735.
- TOWNSEND, A. A. 1980 Sheared turbulence and additional distortion. *J. Fluid Mech.* **98**, 171–191.
- URSELL, F. 1954 Wave generation by wind. In *Surveys in Mechanics* (ed. G. K. Batchelor & R. M. Davis), pp. 216–249. Cambridge University Press.
- ZOU, Q. P. 1998 A viscoelastic model for turbulent flow over undulating topography. *J. Fluid Mech.*, **355**, 81–112.